

Cite this: *Dalton Trans.*, 2023, **52**, 7843

AIE-active cyclometalated iridium(III) complexes for the detection of lipopolysaccharides and wash-free imaging of bacteria†

Aryan Gautam,^a Ajay Gupta,^a Puja Prasad^b and Pijus K. Sasmal *^a

Infectious diseases caused by bacteria pose a major threat to human health and are currently one of the leading causes of mortality worldwide. Therefore, the development of probes for rapid detection of bacteria and their pathogenic components is highly essential. Aggregation-induced emission (AIE)-active compounds have shown great promise for the diagnosis of bacterial infections. In this study, we have synthesized three cationic AIE-active cyclometalated iridium(III) polypyridyl complexes *viz.*, $[\text{Ir}(\text{C}^{\wedge}\text{N})_2(\text{N}^{\wedge}\text{N})]\text{Cl}_2$ (**Ir1–Ir3**), where $\text{C}^{\wedge}\text{N}$ is a cyclometalating ligand such as pq = 2-phenylquinoline (in **Ir1**), pbt = 2-phenylbenzothiazole (in **Ir2**), and dfppy = 2-(2,4-difluorophenyl)pyridine (in **Ir3**), and $\text{N}^{\wedge}\text{N}$ is a 2,2'-bipyridine derivative, for detection of lipopolysaccharide (LPS) in aqueous solution and wash-free imaging of bacteria. These complexes exhibit rapid sensing of LPS also known as endotoxin released by the bacteria, with a detection limit in the nanomolar range being determined by fluorescence spectroscopy within 5 min. Detection of both Gram-negative *Escherichia coli* and Gram-positive *Staphylococcus aureus* bacteria by the complexes is visible to the naked eye and was also observed by fluorescence microscopy imaging. The above features of the complexes make them a promising scaffold for the detection of bacterial contamination in aqueous samples.

Received 28th February 2023,
Accepted 10th May 2023

DOI: 10.1039/d3dt00628j

rsc.li/dalton

Introduction

Infectious diseases caused by bacteria are one of the leading causes of morbidity and mortality worldwide.^{1,2} Therefore, the early and rapid detection of bacterial infections is essential for the clinical diagnosis and prescription of appropriate antibiotics. To detect a bacterial infection, it is possible to detect whole bacteria or their pathogenic components. Lipopolysaccharide (LPS, also commonly known as endotoxin) is a pathogenic component and the main constituent present on the outer cell membranes of Gram-negative bacteria and plays a key role in maintaining the integrity and stability of bacteria and protecting the bacteria against chemical attack.^{2,3} LPS binds strongly with membrane receptor proteins and triggers systemic immune responses in animals which can lead to sepsis, septic shock, endothelial cell destruction, multiorgan dysfunction, and even death in immune-compromised individuals.^{4,5} As a result, the detection of LPS is extremely

important in the manufacture of medical devices, in pharmaceuticals, and in the food industry. Currently, enzymatic limulus amoebocyte lysate (LAL) assay is most commonly used and approved by the FDA for detection and quantification of LPS in clinical samples. Although the LAL assay is a sensitive technique, it requires costly reagents and equipment and the assay is also very sensitive to changes in pH and temperature.^{6,7} On the other hand, the conventional methods for bacterial detection include cell culture, colony counting, polymerase chain reaction, and enzyme-linked immunosorbent assay.^{8,9} In the past few years, some new methods have been reported in the literature for bacterial identification including the use of colorimetric and electrochemical sensors,¹⁰ mass spectrometry,¹¹ surface-enhanced Raman spectroscopy,¹² microfluidic based devices, flow cytometry,⁸ *etc.* However, these methods are generally time-consuming and labor intensive and require expensive equipment, and skilled personnel which limit their practical applications. Therefore, the development of a simple and facile technique for rapid, efficient and sensitive detection of bacteria and their pathogenic components (*e.g.* LPS) is of great importance.

Fluorescent chemical sensors are powerful tools for detecting analytes and are appealing in terms of excellent sensitivity, high accuracy, rapidity, and ease of operation.^{13–15} Recently, several turn-on fluorescent probes have been reported for the

^aSchool of Physical Sciences, Jawaharlal Nehru University, New Delhi 110067, India.
E-mail: pijus@mail.jnu.ac.in

^bAmity Institute of Click Chemistry Research and Studies, Amity University, Noida, Uttar Pradesh 201303, India

† Electronic supplementary information (ESI) available: Methods, characterization data, figures and table. See DOI: <https://doi.org/10.1039/d3dt00628j>

detection of LPS.^{16–21} For example, Wang *et al.* have developed a pair of cationic and anionic fluorescent dyes in a 2 : 1 ratio to detect LPS in aqueous solutions, with the detection limit in the submicromolar concentration range.¹⁶ Xing and co-workers have synthesized magnetic nanoparticles functionalized with a perylene-diimide that conjugated to a LPS-recognition peptide for rapid and selective detection of LPS.¹⁷ The sensitive detection of LPS was also achieved by doubly labeling at the terminal sites of LPS-binding protein CD14 with carboxyfluorescein and tetramethylrhodamine, and the limit of detection (LOD) was about 150 nM.¹⁸

Among the developed turn-on fluorescent probes, the use of aggregation-induced emission luminogens (AIEgens), first discovered by Tang's group in 2001,²² has emerged as a promising method for rapid sensing, imaging, and therapeutic applications.^{23–28} AIEgens are superior over conventional organic fluorescent dyes because of their unique photophysical properties such as high quantum yields, long fluorescence lifetimes, excellent photostability, large Stokes' shifts, no self-quenching, and a light-up response against various analytes. Over the last few years, some organic AIEgens have been developed for the detection of LPS and Gram-negative bacteria.^{29–32} For instance, Hua *et al.* have synthesized a series of near-infrared pyridinium-functionalized dibenzo[*a,c*]phenazine turn-on fluorescent probes with various alkyl chain lengths to detect LPS and Gram-negative bacteria *E. coli*.²⁹ The lowest LOD value achieved with this system for LPS was 26 nM. Niu and co-workers have designed an amphiphilic and positively charged donor–acceptor type AIE probe with a long alkyl chain and one benzenboronic acid substituent for the detection of LPS and the discrimination of Gram-negative bacteria over Gram-positive bacteria.³⁰ The LOD of this system towards LPS was determined to be ~41 nM. In recent years, metal-based AIEgens have gained immense interest because of their varied coordination geometries, structural diversity, rich photophysical properties *etc.* which make them excellent candidates for applications in organic light-emitting diodes, biosensing, bio-imaging and therapy.^{2,33–48} These AIEgen metal complexes can interact with bacteria or their pathogenic components through various noncovalent modes such as electrostatic interactions, hydrogen bonds, van der Waals forces and hydrophobic interactions.² For example, Ding and Yu's groups have developed an AIE-active cationic Pt(II) complex [Pt(N[^]N[^]N)Cl]⁺, where N[^]N[^]N is 2,6-bis(benzimidazol-2'-yl)pyridine with hexaethylene glycol methyl ether groups, which demonstrated sensing of LPS and rapid wash-free discrimination of Gram-negative and Gram-positive bacteria.³⁴ Liu *et al.* have reported AIE-active Zn(II) complexes for selective fluorescence imaging and photoinactivation of bacteria.^{35,36} Among the metal AIEgens, recently, cyclometalated iridium(III) polypyridine complexes have received significant attention for the detection of bacterial pathogenic components (*e.g.* LPS or LTA) and the selective discrimination, imaging, and elimination of Gram-negative and Gram-positive pathogenic bacteria due to their various advantages such as kinetic inertness, positive charge, tunable photophysical and photochemical properties, gene-

ration of high levels of reactive oxygen species, the ease of synthesis, *etc.*^{39–43}

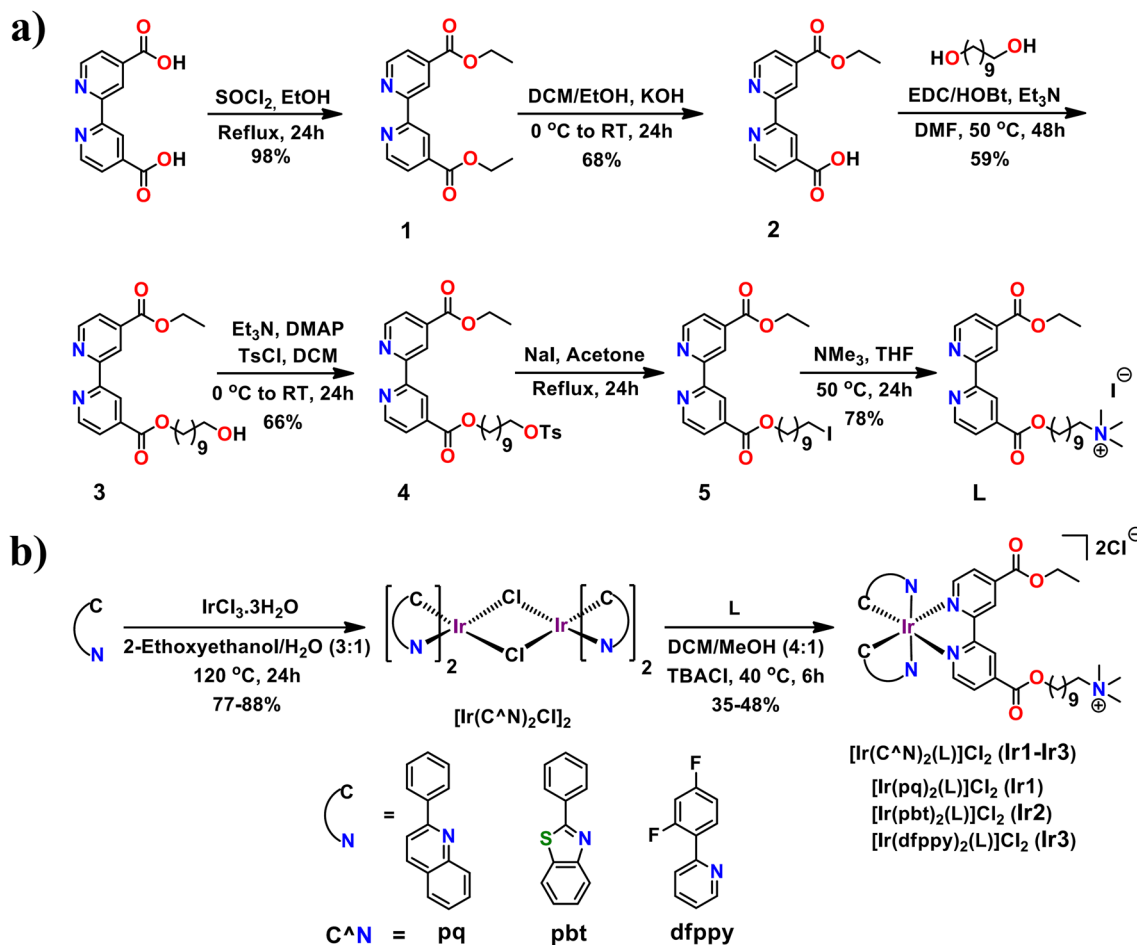
In this work, we have made an effort to develop three cationic AIE-active cyclometalated iridium(III) complexes for rapid detection of bacterial endotoxin (or LPS) in aqueous medium and the wash-free imaging of bacteria (Scheme 1). The complexes can detect endotoxin at a nanomolar concentration within 5 min. Interestingly, the complexes are capable of enabling the detection of both Gram-negative (*E. coli*) and Gram-positive (*S. aureus*) bacteria by the naked eye at a higher concentration of bacteria (10⁸ CFU per ml). However, a lower concentration of bacterial cell (10⁶ CFU per ml) detection with the complexes was also observed by fluorescence spectroscopy. Moreover, the detection of bacteria by the complexes was visualized as well by fluorescence microscopy imaging, which displayed a strong red emission, confirming Ir(III)-complex-mediated cell aggregation. These properties of AIE-active Ir(III) complexes offer great potential for the detection of endotoxin and bacterial contamination in aqueous samples and pharmaceutical products.

Results and discussion

Design, synthesis and characterization of AIE-active cyclometalated iridium(III) complexes

The cyclometalated iridium(III) polypyridyl complexes (**Ir1–Ir3**) were synthesized by the reaction of the bipyridine (N[^]N) ligand with the chloro-bridged cyclometalated (C[^]N) iridium(III) dimers, [Ir(C[^]N)₂Cl]₂ to obtain a stable octahedral geometry of the complexes as shown in Scheme 1. In these complexes, the iridium centres were coordinated with two C[^]N ligands such as phenylquinoline (pq, in **Ir1**), phenylbenzothiazole (pbt, in **Ir2**), and difluorophenylpyridine (dfppy, in **Ir3**) and one bipyridine (N[^]N) ligand, to endow the complexes with AIE properties. The bipyridine ligand in the complexes was conjugated to one ethyl ester and one quaternary ammonium moiety to enhance the aqueous solubility in addition to the increase of the binding affinity of the complexes to the negatively charged LPS and bacterial cell membranes.^{49,50} The synthesized complexes were purified by flash column chromatography and isolated as chloride salts. The characterization of the ligand and the complexes was carried out by NMR, ESI-HRMS, and IR (see Fig. S1–S19†). The iridium(III) complexes were prepared as a mixture of diastereomers. The complexes were found to be soluble in DMSO, DMF, MeCN, DCM, and in an aqueous medium containing 1% DMSO or MeCN at room temperature.

The photophysical properties such as the absorption and emission spectra of the complexes (**Ir1–Ir3**) were studied in water containing 1% DMSO at 298 K (Table 1 and Fig. S20†). The complexes displayed an intense absorption band in the range of 265–365 nm, which can be assigned to the spin-allowed intra-ligand (¹IL) $\pi \rightarrow \pi^*$ transitions for the cyclometalated (C[^]N) and bipyridine (N[^]N) ligands (Table 1 and Fig. S20a†). The less intense absorption bands appeared in the



Scheme 1 Synthetic routes of (a) ligand (L), and (b) cyclometalated iridium(III) polypyridine complexes (Ir1–Ir3). Here, pq = 2-phenylquinoline, pbt = 2-phenylbenzothiazole, and dfppy = 2-(2,4-difluorophenyl)pyridine.

Table 1 Physicochemical data of the cyclometalated iridium(III) polypyridyl complexes (Ir1–Ir3)

Complexes	$\lambda_{\text{abs}}^a/\text{nm}$ ($\epsilon/10^3 \text{ M}^{-1} \text{ cm}^{-1}$)	$\lambda_{\text{em}}^a/\text{nm}$	Φ^b	$\log P_{\text{o/w}}^c$
Ir1	275 (29.2), 315 (16.4), 350 sh (11.9), 430 (3.6)	720	0.033	1.73
Ir2	310 (24.3), 415 (4.9), 500 sh (0.6)	688	0.143	2.28
Ir3	265 (10.8), 310 (6.3), 365 (2.4), 465 (0.3)	640	0.053	1.06

^a Absorption (λ_{abs}) and emission (λ_{em}) spectra of the complexes were recorded in water containing 1% DMSO at 298 K. The emission spectra were measured upon excitation at 425 nm. ^b Quantum yields (Φ) were determined in MeCN at 298 K using $[\text{Ru}(\text{bpy})_3](\text{PF}_6)_2$ ($\Phi = 0.0504$) as the reference. ^c Lipophilicity ($\log P_{\text{o/w}}$) values were determined by measuring the partition coefficient of the complexes in *n*-octanol/water.

range of 415–500 nm were associated with the mixed singlet and triplet metal-to-ligand charge-transfer (¹MLCT and ³MLCT) and ligand-to-ligand charge transfer (LLCT) transitions.^{40,46,47} These complexes showed weak emission in the range of 640–720 nm upon excitation at 425 nm (Table 1 and Fig. S20b†). The complexes **Ir1–Ir3** containing a cyclometalated phenylquinoline (pq) ligand exhibited red shifted emission bands compared to its analogues phenylbenzothiazole (pbt) and difluorophenylpyridine (dfppy). The emission intensity did not vary significantly with the increase in the concentrations of these iridium complexes (Fig. S21†). The quantum

yields (Φ) of the complexes were determined in MeCN at 298 K, and they lie between 0.033 and 0.143 (Table 1). The emission properties of these complexes have been utilized to detect LPS and bacteria.

Investigation of AIE phenomena of the iridium(III) complexes

To investigate the AIE properties, the emission intensity of the cyclometalated iridium(III) complexes was measured in a water–THF mixture by fluorescence spectroscopy. Since the complexes are less soluble in THF, the increase in the percentage of THF in a water–THF mixture induces the aggregation of

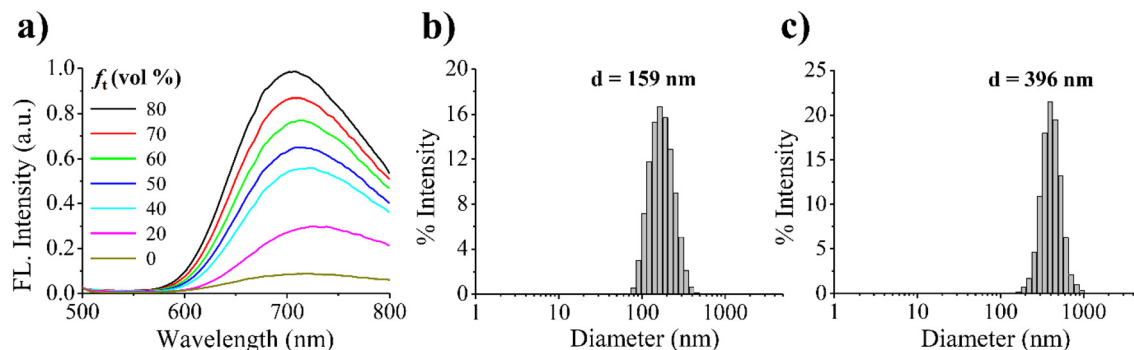


Fig. 1 (a) Emission spectra of **Ir1** (50 μM) recorded in a water–THF mixture with different THF fractions (f_t). Hydrodynamic diameter (d) and particle size distribution of complex **Ir1** (50 μM) (b) in the absence, and (c) in the presence of 25% THF in a water–THF mixture.

the complexes in water. The fluorescence spectroscopy studies showed that the complexes were weakly emissive in the range of 640–720 nm ($\lambda_{\text{ex}} = 425$ nm) in aqueous solution, and the emission intensity of the complexes gradually increased after the addition of THF fraction from 0 to 80% in the mixed solution (Fig. 1a and S22†). As the amount of THF in the mixed solution increases, aggregated particles are formed. The simultaneous enhancement in the emission intensity and the shift in the emission maxima of the complexes suggest their unique AIE phenomenon.^{40,47} Furthermore, the aggregation behaviors of the complexes were confirmed and characterized by determining the hydrodynamic diameter of the complexes in the absence and presence of THF by dynamic light scattering (DLS) studies (Fig. 1b, c and S23–25†). For instance, the hydrodynamic diameter of **Ir1** in the absence of THF was 159 nm (Fig. 1b and S23†); however, its diameter increased significantly to 396 nm, and 431 nm when 25%, and 50% THF were present, respectively in the water–THF mixture (Fig. 1c and S23†). Notably, it was observed that **Ir1** showed better aggregation capability compared to **Ir2** and **Ir3** in the water–THF mixture (Fig. S23–25†).

Detection of bacterial endotoxin

The unique AIE properties of the iridium(III) complexes (**Ir1**–**Ir3**) were exploited for the detection of bacterial pathogenic components such as LPS or endotoxin. For this, the complexes were titrated with LPS in aqueous media at ambient temperature, and its phosphorescence intensity was recorded after 2 min (Fig. 2 and S26–28†). Initially, before the addition of LPS, complex **Ir1** in aqueous solution was weakly emissive. However, upon gradual addition of LPS, the emission intensity of the complex increased in the range of 550–800 nm with somewhat a blue shift of ~ 40 nm (Fig. 2a). Such a blue-shifted emission is due to the formation of LPS–Ir(III) aggregates, leading to the development of a non-polar microenvironment.³⁰ Fig. 2b shows the plot of emission intensity of complex **Ir1** at 720 nm with different LPS concentrations ranging from 0 to 3 μM which displayed a linear relationship ($R^2 = 0.954$) up to 0.8 μM . The limit of detection (LOD) of LPS is determined to be 47 nM using the formula $C_{\text{LOD}} = 3\sigma/S$ (where σ is the standard deviation (SD) obtained from six independent readings of emission intensity of the **Ir1** complex in

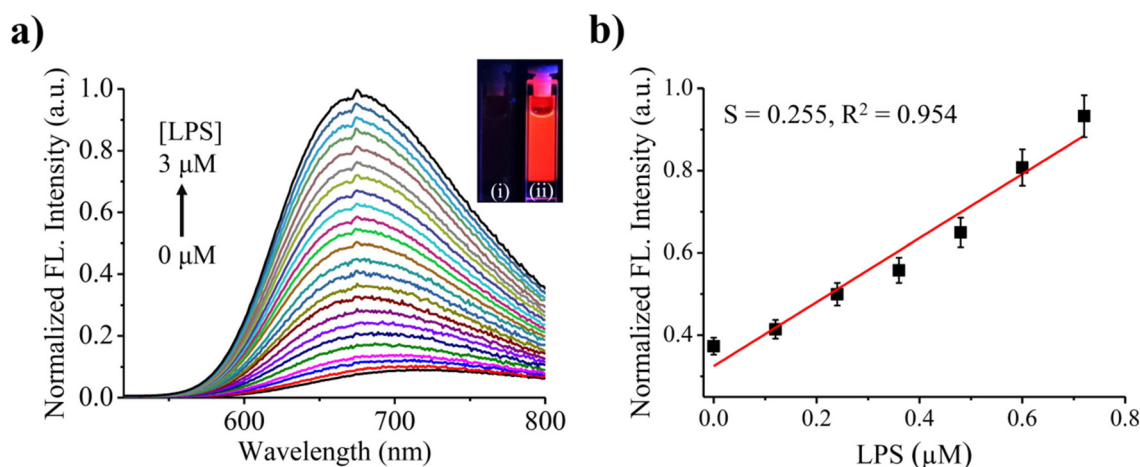


Fig. 2 (a) Emission titration spectra of complex **Ir1** (50 μM) upon gradual addition of LPS (0–3 μM). The inset shows the phosphorescent emission images of complex **Ir1** (50 μM) at room temperature under 365 nm UV lamp illumination in the (i) absence and (ii) presence of LPS (3 μM). (b) The plot and linear fitting of the emission intensity of **Ir1** at 720 nm with different concentrations of LPS (0 to 0.8 μM).

aqueous media without any LPS and S is the slope obtained after linear fitting of the titration curves). The LOD of complexes **Ir2** and **Ir3** with LPS was estimated to be 144 nM and 157 nM, respectively (Table S1 and Fig. S27, S28†). The LOD of **Ir2** and **Ir3** is higher than that of **Ir1** which could be due to their poor aggregation with LPS as determined by DLS studies (Fig. S29†). This observation is also corroborated by the weak aggregation properties of the **Ir2** and **Ir3** complexes than those of **Ir1** in the water-THF mixture studied by DLS (Fig. S23–25†). The LOD of these complexes is comparable to or lower than previously reported systems in the literature.^{16–19,21,29,30} Our iridium complexes are bearing with doubly positive charges, and hence they can interact strongly with negatively charged LPS through electrostatic interactions leading to the formation of LPS-Ir(III) aggregates. An increase in the phosphorescence intensity of the complexes **Ir1–Ir3** was attributed to triplet metal-to-metal-to-ligand charge-transfer (³MMLCT), which originates from the strong intermolecular π - π stacking interactions involving C^N and N^N ligands attached to the Ir(III) center due to the formation of LPS-Ir(III) aggregates.

The formation of LPS-Ir(III) aggregates was further corroborated by DLS studies and transmission electron microscopy (TEM) imaging (Fig. 3 and S29, S30†). An increase in the hydrodynamic diameter of the complexes after addition of LPS was determined by DLS, confirming the formation of aggregates due to the electrostatic interaction between the positively charged Ir(III) complex and the negatively charged LPS (Fig. S29†). Direct evidence of binding of the complexes to LPS was provided by TEM, which exhibited that the complex was substantially more aggregated in the presence of LPS (Fig. 3 and S30†). We believe that the formation of aggregates can be caused *via* electrostatic interaction between the cationic Ir(III) complexes having a quaternary ammonium moiety and negatively charged phosphate or carboxylic groups on the LPS molecules. Furthermore, this interaction is facilitated by the hydrophobic interactions of an alkyl linker present in between the N^N donor bipyridyl moiety and the quaternary ammonium group in the Ir(III) complexes with the alkyl chains in LPS.

In order to explore the practical applicability of the Ir(III) complexes for endotoxin detection under real conditions, we studied the effect of pH on the complexes in the absence or presence of LPS. The phosphorescence intensity of the complexes in the absence of LPS showed no significant change in a wide range of pH from 4 to 9, implying the good stability of the Ir(III) probes and their reliability for LPS detection (Fig. 4 and S31†). The phosphorescence intensity of the complexes **Ir1** and **Ir2** was enhanced in the presence of LPS between pH 4 and 9. However, under acidic conditions of pH 4, we observed that there is a slight decrease in the phosphorescence intensity of both the complexes in the presence of LPS. This may be due to the protonation of negatively charged groups such as carboxylate and phosphate groups present on LPS at acidic pH which weaken its electrostatic interaction with the cationic Ir(III) complexes, leading to loose packing of aggregates and thereby decreasing the phosphorescence intensity.³⁰

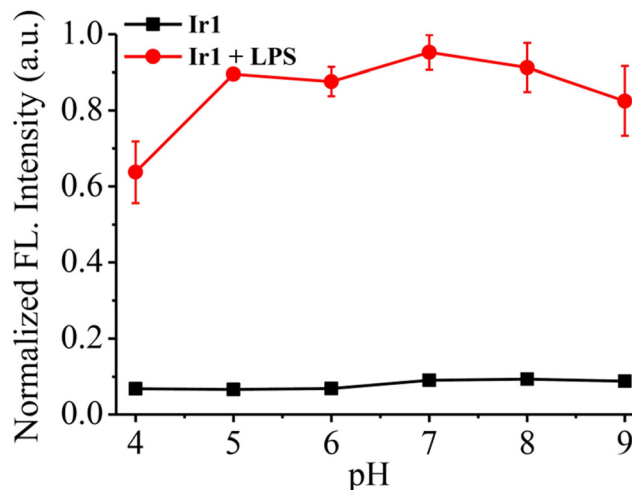


Fig. 4 The emission intensity of **Ir1** (50 μ M) at 720 nm in 10 mM HEPES buffer in the absence (■) and presence (●) of LPS (6 μ M) in different pH solutions at room temperature.

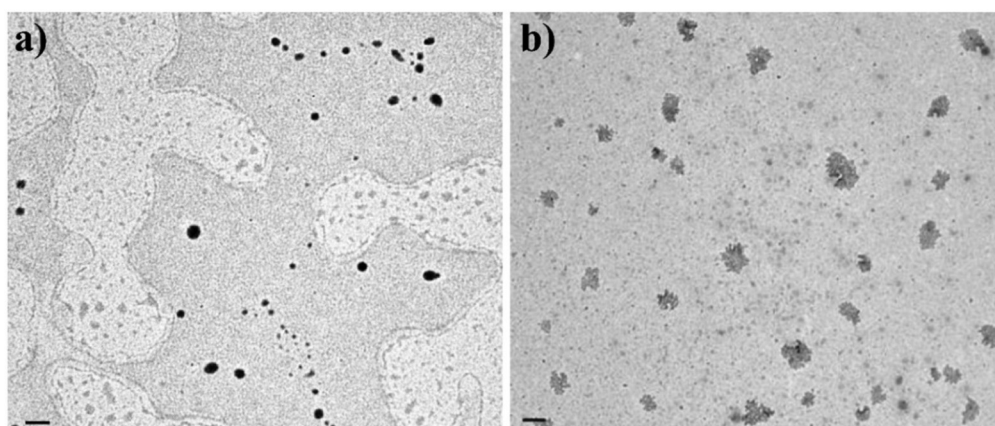


Fig. 3 TEM images of complex **Ir2** (50 μ M) in water containing 1% MeCN in the (a) absence and (b) presence of 3 μ M LPS. Scale bar: 100 nm.

Bacterial detection with the naked eye and fluorescence spectroscopy

Before proceeding with bacterial detection studies, we first determined the lipophilicity index of our AIE-active iridium complexes since the lipophilicity of the complexes plays a crucial role in the uptake of drugs in the cells.^{40,47} Hence, the lipophilicity ($\log P_{o/w}$: partition coefficient in *n*-octanol/water system) values of the complexes were calculated by the classical flask-shaking technique. The $\log P_{o/w}$ values of the complexes lie in the range of 1.06–2.28, suggesting their quite lipophilic character (Table 1). Next, we checked the detection capability of bacteria by our iridium(III) complexes. The rapid detection of pathogenic bacteria is important in clinical diagnosis and the establishment of therapeutic strategies. So far, we have seen that our cationic Ir(III) complexes can detect the bacterial LPS. Nevertheless, these LPSs are present in approximately one million copies per cell on the outer wall of all Gram-negative bacteria. Targeting these naturally amplified biomarker by our Ir(III) complexes could induce strong AIE that would help to detect different Gram-negative bacteria. Notably, the detection of whole bacteria by these complexes can be visualized by the naked eye. Upon addition of 400 μM of the Ir1 complex to 10^8 CFU per ml of Gram-negative bacteria (*E. coli*), we found bacteria agglutinated immediately which was clearly visible by the naked eye within 5 min and then precipitated out after 2 h (Fig. 5a). Furthermore, the detection of bacteria

by our complexes can also be observed at a lower concentration to 10^6 CFU per ml by using fluorescence spectroscopy. For this, different concentrations of bacteria (0, 10^5 , 10^6 , 10^7 , and 10^8 CFU per ml) were prepared and treated with the Ir1 complex. The results showed that 1- and 1.5-fold increases in the phosphorescence intensity of Ir1 were determined with 10^5 and 10^6 CFU per ml bacterial population, respectively, compared to the control (iridium complex only). However, the intensity is significantly increased to 5- and 10-fold with 10^7 and 10^8 CFU per ml bacteria, respectively, and is better than those of reported systems (Fig. 5b).^{19,20} This was further verified with another experiment where the bacteria at different concentrations were treated with the iridium complex and then the sample was observed under UV light of 365 nm. A red fluorescence of the bacteria treated with the complex was noticed by the naked eye, indicating iridium-mediated bacterial cell aggregation (Fig. 5c). We have also explored these cyclometalated iridium(III) complexes for the detection of Gram-positive bacteria. A similar observation was found when the experiments were repeated with Gram-positive bacteria *S. aureus*.

Bacterial detection by optical microscopy

The agglutination of bacteria with the Ir(III) complexes was further verified and confirmed by optical microscopy. For this study, the resistant strains of Gram-negative (*E. coli*) and

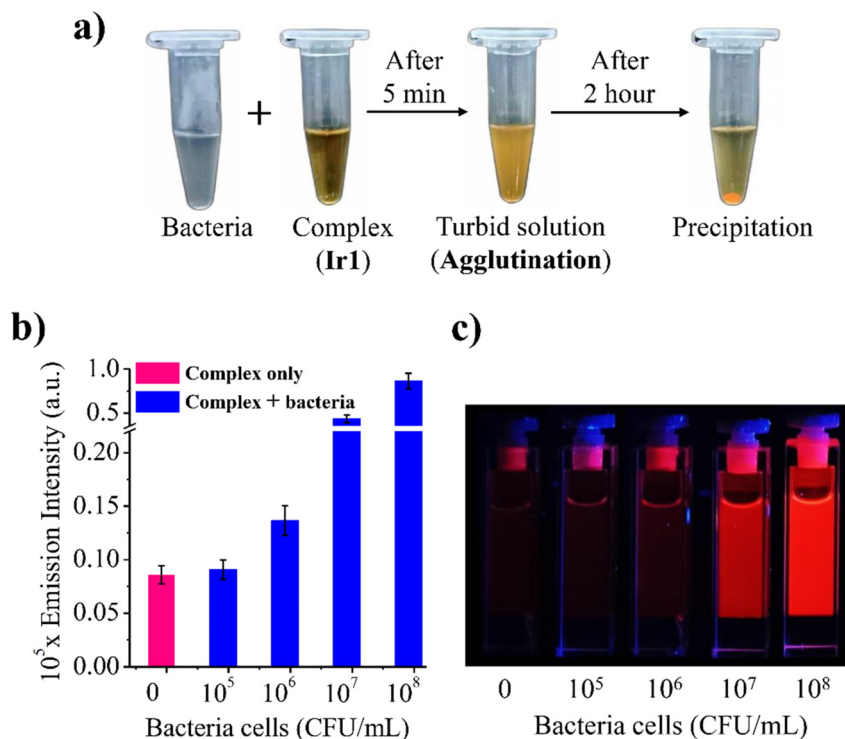


Fig. 5 Bacterial agglutination tests in a spiked water sample visualized by (a) the naked eye, (b) fluorescence spectroscopy, and (c) under 365 nm UV lamp illumination. (a) 10^8 CFU per ml of *E. coli* was treated with 400 μM of complex Ir1. (b) Different concentrations (10^5 – 10^8 CFU per ml) of *E. coli* were treated with 50 μM of complex Ir1 and its phosphorescence intensity was measured after 5 min. (c) Phosphorescent emission images of 50 μM of complex Ir1 with different bacterial cells (10^5 – 10^8 CFU per ml) recorded under illumination with a 365 nm UV lamp.

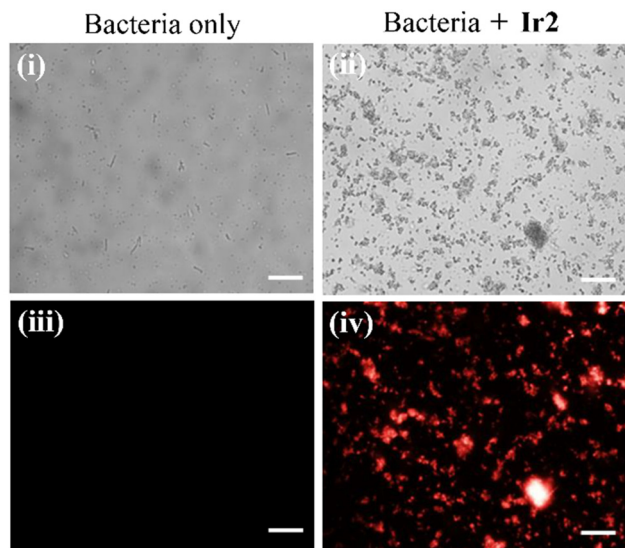


Fig. 6 Optical microscopy images of *S. aureus* (10^8 CFU per ml) after incubation with $400 \mu\text{M}$ of complex **Ir2** and the results were observed in complementary bright-field (i and ii) and fluorescence (iii and iv) modes. Here, left panels (i and iii) indicate the results for bacteria only and right panels (ii and iv) for bacteria treated with complex **Ir2**. Scale bar: $5 \mu\text{m}$.

Gram-positive (*S. aureus*) bacteria when incubated with the Ir(III) complexes for 5 min displayed a strong red emission which was clearly visualized under a fluorescence microscope (Fig. 6 and S32†). Whereas, the bacteria without the Ir(III) complex appeared as blank (Fig. 6(i and iii)). The bright- and dark-field images showed small and large aggregates of Ir(III)-complex-mediated cell agglutination which leads to the AIE phenomena (Fig. 6(ii and iv)). Fluorescence imaging of the bacteria using the AIE-characteristic Ir(III) probes showed no background noise and its high photostability even after increasing the exposure time. In this method, the bacteria were clearly visible without any washing procedure, which decreases the bacterial loss during the washing process, resulting in a higher accuracy of bacterial detection and simplifies the imaging process.⁵¹ Hence, the above properties of AIE-active Ir(III) complexes make them suitable and advantageous over conventional fluorescence dyes for imaging of bacteria.

Conclusions

In conclusion, we have synthesized three cationic AIE-active cyclometalated iridium(III) complexes for rapid detection of wash-free bacteria and their pathogenic components such as LPS in aqueous solutions. The complexes were appended with a cationic quaternary ammonium group to enhance their aqueous solubility and to increase their binding affinity with the negatively charged LPS and bacterial cell membranes. These complexes exhibit rapid sensing of bacterial LPS (or endotoxin) at a nanomolar concentration within 5 min through AIE phenomena. The aggregation of the complexes with LPS was confirmed by DLS and TEM imaging studies.

Interestingly, the detection of both Gram-negative (*E. coli*) and Gram-positive (*S. aureus*) bacteria by the complexes was achieved with the naked eye at a higher bacterial concentration (10^8 CFU per ml). Moreover, these complexes were also capable of detecting lower bacterial concentrations (10^6 CFU per ml) by fluorescence spectroscopy. Moreover, these complexes can image bacteria without the involvement of the washing procedure which were visualized under a fluorescence microscope, showing a strong red emission of the bacterial cells upon incubation with the Ir(III) complexes. Our studies revealed that these AIE-active iridium(III) complexes could be useful for the detection of LPS and bacterial contamination in aqueous samples, pharmaceuticals and food products.

Experimental section

Materials

Solvents were distilled under nitrogen from calcium chloride (CH_2Cl_2), magnesium chips (MeOH), sodium/benzophenone (THF) or calcium hydride (acetone). All reactions were carried out under an argon atmosphere. 2-Phenylquinoline (pq), 2-(2,4-difluorophenyl)pyridine (dfppy), 2,2'-bipyridine-4,4'-dicarboxylic acid, 2-aminothiophenol, triethylamine, tetrabutylammonium chloride (TBACl), 1,10-decanediol, and 4-(2-hydroxyethyl)-1-piperazineethanesulfonic acid (HEPES) were purchased from Sigma-Aldrich. $\text{IrCl}_3 \cdot 3\text{H}_2\text{O}$ and 4-dimethylaminopyridine (DMAP) were obtained from Alfa-Aesar and trimethylamine (13% in tetrahydrofuran, 2 mol l^{-1}) was procured from Tokyo Chemical Industry (TCI). 1-Ethyl-3-(3 dimethylaminopropyl)carbodiimide (EDC), 1-hydroxybenzotriazole hydrate (HOBT), benzoyl chloride, potassium hydroxide, sodium iodide, *p*-toluenesulfonyl chloride and thionyl chloride were purchased from Central Drug House (CDH). Thin layer chromatography (TLC) was sourced from Merck, Germany. Cyclometalated ligand **pbt** and compounds **1** and **2** and the chloro-bridged cyclometalated iridium(III) dimers were synthesized according to a method reported in the literature.⁴⁷ The purity of the synthesized iridium(III) complexes (**Ir1–Ir3**) used for sensing application was found to be $\geq 95\%$ by NMR and high resolution mass spectrometry.

Synthesis of compound 2

compound **1** (50 mg, 0.185 mmol) was placed in an oven-dried round bottom-flask and dissolved in dry DCM (7 ml) under an argon atmosphere. To this, KOH (10.37 mg, 0.185 mmol) in dry EtOH (1.8 ml) was added in a dropwise manner over a period of 30 min at 0°C . The resulting mixture was stirred at room temperature for 24 h and a white precipitate was obtained. The precipitate was collected by filtration and washed with EtOAc to remove the unreacted compound **1**. The precipitate was dissolved in water. The pH of the above solution was maintained at 3 by adding 1 N HCl to obtain a white precipitate of the product. The product was collected by filtration and dried under vacuum (yield: 68%).

^1H NMR (500 MHz, DMSO- d_6) δ (ppm) 13.91 (br, 1H), 8.89 (t, $J = 4.2$ Hz, 2H), 8.79 (m, 2H), 7.89 (d, $J = 4.5$ Hz, 2H), 4.39 (q, $J = 7.0$ Hz, 2H), 1.36 (t, $J = 7.0$ Hz, 3H). ^{13}C -NMR (125 MHz, DMSO- d_6): δ (ppm) 166.45, 164.91, 155.96, 155.73, 151.19, 151.08, 139.97, 138.86, 124.02, 123.69, 120.02, 119.60, 62.25, 14.50. IR (ATR) ν (cm^{-1}): 3336 br (O–H), 2900 m (C–H: aliphatic), 1728 vs (C=O, ester), 1706 s (C=O, acid), 1598 w, 1460 m, 1284 s, 1232 s, 1139 m, 1016 s, 912 m, 862 m, 761 s, 661 m. ESI-HRMS (m/z): calculated 273.0875 $[\text{M} + \text{H}]^+$, found 273.0862.

Synthesis of compound 3

Compound 2 (50 mg, 0.184 mmol), EDC (45.7 mg, 0.239 mmol) and HOBt (42.1 mg, 0.276 mmol) were dissolved in DMF (600 μl). The reaction mixture was stirred at room temperature under an argon atmosphere for 30 min. After that 1,10-decanediol (41.6 mg, 0.239 mmol) and triethylamine (128 μl , 0.918 mmol) were added to the above reaction mixture and stirred at 50 $^\circ\text{C}$ for 48 h. The reaction mixture was cooled to room temperature and diluted with water (10 ml) followed by extraction with CH_2Cl_2 (3 \times 20 ml). The combined organic phases were washed with brine and dried over Na_2SO_4 . The organic phase was evaporated on a rotary evaporator to give a yellowish oily crude material. The crude material was purified by column chromatography on silica gel using hexane/EtOAc (2 : 1, v/v) as the eluent to yield an off-white product (yield: 59%).

^1H -NMR (500 MHz, CDCl_3): δ (ppm) 8.94 (s, 2H), 8.86 (d, $J = 5.0$ Hz, 2H), 7.90 (m, 2H), 4.46 (q, $J = 7.0$ Hz, 2H), 4.39 (t, $J = 6.2$ Hz, 2H), 3.63 (t, $J = 6.5$ Hz, 2H), 1.81 (m, 2H), 1.55 (m, 2H), 1.43 (m, 5H), 1.34–1.30 (m, 10H). ^{13}C -NMR (125 MHz, CDCl_3): δ (ppm) 165.35, 165.28, 156.67, 156.65, 150.20, 139.14, 139.12, 123.36, 123.35, 120.72, 120.70, 66.17, 63.13, 62.03, 32.88, 29.59, 29.51, 29.49, 29.32, 28.72, 26.04, 25.84, 14.39. IR (ATR) ν (cm^{-1}): 3415 br (O–H), 2918 m (C–H: aliphatic), 2850 m, 1715 vs (C=O), 1593 m, 1471 m, 1355 m, 1292 m, 1244 m, 1132 s, 1031 w, 952 m, 871 m, 759 s, 698 m.

Synthesis of compound 4

Compound 3 (41 mg, 0.096 mmol), triethylamine (67 μl , 0.479 mmol) and a catalytic amount of DMAP were dissolved in 1 ml of dry DCM. The reaction mixture was stirred under an argon atmosphere at 0 $^\circ\text{C}$ for 10 min. After this, tosyl chloride (91.3 mg, 0.479 mmol) was dissolved in dry DCM (500 μl) and added to the above reaction mixture in a dropwise manner at 0 $^\circ\text{C}$. The resulting mixture was stirred for 24 h at room temperature. After completion of the reaction, the mixture was diluted with DCM and washed with 0.1 M HCl (3 \times 15 ml), followed by brine and dried over Na_2SO_4 . The organic phase was evaporated on a rotary evaporator to give a pale yellowish oily crude material, which was purified by column chromatography on silica gel using DCM/MeOH (20 : 1, v/v) as the eluent to yield a pale yellowish oily product (yield: 66%).

^1H -NMR (500 MHz, CDCl_3): δ (ppm) 8.94 (s, 2H), 8.87 (d, $J = 4.5$ Hz, 2H), 7.91 (m, 2H), 7.78 (d, $J = 8.0$ Hz, 2H), 7.34 (d, $J = 8.5$ Hz, 2H), 4.46 (q, $J = 7.5$ Hz, 2H), 4.38 (t, $J = 7.0$ Hz, 2H),

4.01 (t, $J = 6.5$ Hz, 2H), 2.44 (s, 3H), 1.80 (m, 2H), 1.62 (m, 4H), 1.43 (m, 5H), 1.37–1.28 (m, 9H). ^{13}C -NMR (125 MHz, CDCl_3): δ (ppm) 165.34, 165.27, 156.71, 156.68, 150.20, 144.70, 139.14, 133.49, 129.90, 129.69, 127.99, 127.17, 123.34, 120.69, 70.76, 66.12, 62.00, 42.12, 29.43, 29.39, 29.29, 29.00, 28.95, 28.74, 26.03, 25.44, 21.72, 14.39. IR (ATR) ν (cm^{-1}): 2923 m (C–H: aliphatic), 1716 vs (C=O), 1543 m, 1361 s, 1292 s, 1176 m, 1130 m, 1095 w, 964 m, 810 w, 763 m, 694 w, 667 m.

Synthesis of compound 5

Compound 4 (35 mg, 0.060 mmol) and sodium iodide (45 mg, 0.300 mmol) were taken in a round bottom flask and dissolved in dry acetone (1.5 ml). The solution was refluxed under an argon atmosphere for 24 h. After completion, the reaction mixture was cooled to room temperature and dried under high vacuum. The dried mixture was dissolved in DCM and washed with water (2 \times 15 ml) and brine. The organic layer was dried over MgSO_4 and the solvent was evaporated to dryness to obtain a pale yellowish oily crude material. The crude material was purified by column chromatography on silica gel using hexane/EtOAc (5 : 1, v/v) as the eluent to yield a pale yellowish oily product. The compound 5 was used directly in the next step without characterization.

Synthesis of compound L

A solution of compound 5 (25 mg, 0.046 mmol) in dry THF (1 ml) was placed in a round bottom flask under an argon atmosphere. To the above solution, trimethylamine (111 μl) in 0.5 mL of THF was added in a dropwise manner and then the mixture was stirred at 50 $^\circ\text{C}$ for 24 h. After completion, the reaction mixture was cooled to room temperature and dried under high vacuum to remove the excess of trimethylamine to give a crude material. The crude product was washed with diethyl ether (3 \times 4 ml) and dried in a vacuum to obtain an off-white powder (yield: 78%).

^1H -NMR (500 MHz, CDCl_3): δ (ppm) 8.93 (s, 2H), 8.86 (m, 2H), 7.91 (m, 2H), 4.45 (q, $J = 7.0$ Hz, 2H), 4.38 (t, $J = 6.8$ Hz, 2H), 3.59 (m, 2H), 3.45 (s, 9H), 1.78 (m, 4H), 1.44 (m, 5H), 1.36–1.29 (m, 10H). ^{13}C -NMR (125 MHz, CDCl_3): δ (ppm) 165.25, 165.18, 150.18, 139.05, 123.34, 123.31, 120.58, 67.22, 66.08, 61.99, 53.82, 29.30, 29.29, 29.18, 29.16, 28.62, 26.08, 25.91, 23.24, 14.32. IR (ATR) ν (cm^{-1}): 2925 m (C–H: aliphatic), 1724 vs (C=O), 1593 m, 1556 m, 1367 s, 1284 s, 1259 s, 1244 s, 1134 s, 1062 w, 1018 m, 763 s, 725 m, 692 m. ESI-HRMS (m/z): calculated 470.3013 $[\text{M}]^+$, found 470.2504.

General procedure for the synthesis of complexes Ir1–Ir3

The iridium(III) dimer, $[\text{Ir}(\text{C}^{\wedge}\text{N})_2\text{Cl}]_2$ (0.015 mmol) and the $\text{N}^{\wedge}\text{N}$ donor bipyridine ligand (L, 0.033 mmol) were placed in an oven-dried round bottom-flask under an argon atmosphere. To this, degassed $\text{CH}_2\text{Cl}_2/\text{MeOH}$ (1.5 ml; 4 : 1 v/v) was introduced and the resulting mixture was heated at 40 $^\circ\text{C}$ and stirred for 6 h. Subsequently, the solution was cooled to room temperature, followed by treated with a large excess of tetrabutylammonium chloride (TBACl) and then stirred for 15 min for accomplishing counterion metathesis. The solvent was

removed on a rotary evaporator and the resulting solid was washed with diethyl ether (3 × 5 ml). The crude material was purified by preparative thin layer chromatography using CH₂Cl₂/MeOH (20 : 1, v/v) and the product was dried under vacuum to afford the corresponding complex.

Ir1 yield: 48%

¹H NMR (400 MHz, CDCl₃) δ (ppm) 8.58 (d, *J* = 6.0 Hz, 2H), 8.45 (m, 2H), 8.41 (d, *J* = 6.0 Hz, 1H), 8.33 (m, 2H), 8.24 (d, *J* = 8.8 Hz, 1H), 8.11 (m, 2H), 8.04 (m, 2H), 7.86 (d, *J* = 6.8 Hz, 1H), 7.77 (d, *J* = 6.8 Hz, 1H), 7.39 (m, 2H), 7.19 (m, 2H), 7.12 (t, *J* = 8.0 Hz, 2H), 7.00 (m, 2H), 6.83 (m, 2H), 6.52 (d, *J* = 7.2 Hz, 1H), 6.47 (d, *J* = 7.2 Hz, 1H), 4.44 (q, *J* = 7.2 Hz, 2H), 4.36 (t, *J* = 6.4 Hz, 2H), 3.75 (m, 2H), 3.42 (s, 9H), 1.75 (m, 5H), 1.41 (m, 5H), 1.32–1.27 (m, 9H). ¹³C-NMR (125 MHz, CDCl₃): δ (ppm) 169.65, 169.59, 162.84, 162.63, 155.80, 155.56, 149.52, 149.20, 149.11, 148.89, 147.15, 147.10, 145.15, 145.13, 140.92, 140.60, 140.16, 140.11, 134.67, 134.46, 131.59, 131.30, 129.86, 129.59, 127.84, 127.72, 127.68, 127.64, 127.42, 127.31, 127.26, 127.08, 124.18, 124.02, 123.85, 123.69, 123.18, 123.07, 118.25, 117.84, 67.50, 66.72, 63.38, 54.05, 29.71, 29.03, 29.00, 28.96, 28.92, 28.39, 25.81, 23.24, 14.24. IR (ATR) ν (cm⁻¹): 2920 s (C–H: aliphatic), 2850 m, 1724 vs (C=O), 1604 m, 1579 m, 1516 m, 1463 m, 1404 m, 1294 m, 1249 s, 1232 s, 1072 m, 916 m, 763 vs, 721 vs, 659 m. ESI-HRMS (*m/z*): calculated 535.7132 [M]²⁺, found 535.7583.

Ir2 yield: 38%

¹H NMR (500 MHz, CDCl₃) δ (ppm) 8.99 (s, 2H), 8.36 (d, *J* = 6 Hz, 1H), 8.32 (d, *J* = 5.5 Hz, 1H), 8.21 (dd, *J* = 6 Hz, 1.5 Hz, 1H), 8.12 (dd, *J* = 5.5, 1.5 Hz, 1H), 8.03 (d, *J* = 8.0 Hz, 1H), 7.93 (d, *J* = 8.0 Hz, 1H), 7.86 (m, 2H), 7.41 (m, 2H), 7.15 (m, 4H), 6.91 (m, 2H), 6.36 (d, 7.5 Hz, 1H), 6.33 (d, 7.5 Hz, 1H), 6.11 (dd, *J* = 14.0, 8.4 Hz, 2H), 4.52 (q, *J* = 7.5 Hz, 2H), 4.45 (t, *J* = 6.5 Hz, 2H), 3.74 (m, 2H), 3.41 (s, 9H), 1.80 (m, 4H), 1.44 (m, 5H), 1.37–1.28 (m, 10H). ¹³C-NMR (125 MHz, CDCl₃): δ (ppm) 181.52, 181.29, 163.23, 162.99, 162.73, 157.03, 156.68, 152.30, 151.89, 148.92, 148.87, 148.39, 141.00, 140.93, 140.65, 139.88, 139.86, 133.48, 133.31, 132.78, 132.74, 131.60, 131.35, 128.93, 128.69, 128.63, 128.24, 127.29, 127.01, 126.73, 126.60, 124.51, 124.23, 124.08, 124.03, 123.94, 117.24, 116.96, 67.74, 66.83, 63.66, 54.21, 32.05, 29.82, 28.97, 28.88, 28.56, 25.90, 25.76, 23.31, 14.42. IR (ATR) ν (cm⁻¹): 2920 m (C–H: aliphatic), 2850 m, 1722 s (C=O), 1645 m, 1579 w, 1467 m, 1406 m, 1319 w, 1298 w, 1265 m, 1024 w, 758 s. ESI-HRMS (*m/z*): calculated 541.6696 [M]²⁺, found 541.7126.

Ir3 yield: 35%

¹H NMR (500 MHz, CDCl₃) δ (ppm) 9.15 (s, 1H), 8.93 (s, 1H), 8.85 (d, *J* = 4.5 Hz, 1H), 8.30 (m, 2H), 8.17 (m, 2H), 8.09 (m, 2H), 7.88 (m, 3H), 7.65 (m, 2H), 6.59 (t, *J* = 10.2 Hz, 2H), 5.65 (d, *J* = 8.0 Hz, 2H), 4.48 (m, 4H), 3.59 (m, 2H), 3.37 (s, 9H), 1.841.76 (m, 3H), 1.44 (m, 6H), 1.38–1.32 (m, 10H). ¹³C-NMR (125 MHz, CDCl₃): δ (ppm) 165.37, 165.30, 163.94, 163.82, 162.94, 162.77, 156.67, 156.23, 156.07, 152.45, 152.32, 151.73, 151.50, 150.23, 149.43, 149.23, 141.24, 139.89, 139.11, 130.03,

128.75, 128.56, 127.49, 125.07, 124.73, 124.54, 124.23, 124.03, 123.38, 120.69, 114.25, 114.07, 100.16, 99.94, 66.12, 63.50, 62.05, 53.57, 29.82, 29.37, 28.92, 28.70, 28.57, 25.98, 23.34, 22.81, 14.40. IR (ATR) ν (cm⁻¹): 2925 m (C–H: aliphatic), 2852 m, 1724 s (C=O), 1607 s, 1560 m, 1477 m, 1429 w, 1406 m, 1319 w, 1234 s, 1164 w, 1105 s, 1068 w, 989 m, 829 m, 763 m, 721 m. ESI-HRMS (*m/z*): calculated 521.6787 [M]²⁺, found 521.7153.

UV-visible spectra

The absorption spectra of the cyclometalated iridium(III) complexes (**Ir1–Ir3**) were measured in water containing 1% DMSO at room temperature. All UV-vis spectroscopic measurements were performed in a quartz cuvette with an optical path length of 10 mm and the wavelength was reported in nanometers (nm).

Emission spectra and determination of quantum yield

Emission spectra of the **Ir1–Ir3** complexes (50 μM) were measured in water containing 1% DMSO at 298 K. The emission spectra were recorded using a quartz cuvette with an optical path length of 10 mm. The wavelength of excitation used for all the complexes was 425 nm, and both slits were set to 5 nm for the emission spectra. Quantum yields (Φ) were studied in MeCN at room temperature using [Ru(bpy)₃](PF₆)₂ (Φ = 0.0504) as the reference. Briefly, the absorbance values of the solutions ([Ru(bpy)₃](PF₆)₂ and the iridium complexes) at different concentrations were determined at their respective excitation wavelengths by using a UV-vis spectrophotometer. Similarly, the emission spectra of all the solutions at different concentrations of the complexes were measured at their excitation wavelengths. Then the quantum yields were calculated by determining the area under the curve by using the following formula: $\Phi = \Phi_R [G/G_R] [\eta^2/\eta_R^2]$, where, Φ is the quantum yield, G is the gradient obtained from the plot of integrated fluorescence intensity vs. absorbance, and η is the refractive index of the solvent (for MeCN = 1.34). The subscript R refers to the standard fluorophore of the known quantum yield ([Ru(bpy)₃](PF₆)₂ in our case).

Aggregation-induced emission studies

The iridium complexes (**Ir1–Ir3**) of 50 μM concentration were prepared in 1% v/v DMSO in water with a total volume of 2 ml. The complexes were titrated with different amounts of THF at room temperature and their phosphorescence emission spectra were measured. The hydrodynamic diameters (*d*) of the complexes (**Ir1–Ir3**) in water and their aggregated particles in water–THF mixtures were determined by DLS.

Determination of lipophilicity

The lipophilicity ($\log P_{o/w}$) of the iridium(III) complexes (**Ir1–Ir3**) was determined by the classical flask-shaking method as per the literature report.⁴⁰ Here, $\log P_{o/w} = \log(C_o/C_w)$ is defined as the logarithmic ratio of the complex concentration in *n*-octanol to that in the water phase. Accordingly, 0.5 mg of the complexes was added into 3 ml of a 1:1 v/v mixture of

n-octanol and water, and mixed vigorously for 24 h. Then the mixture was kept in a stationary state for an additional 24 h to reach saturation. After that *n*-octanol and water phases were separated and centrifuged at 3000 rpm for 10 min and the supernatant was isolated. The concentration of the complexes was then determined by UV-vis spectroscopy in both the *n*-octanol (C_o) and water (C_w) phases to determine the $\log P_{o/w}$ values.

Determination of the limit of detection of LPS

The solution of the iridium complexes (50 μ M) was prepared in water containing 1% DMSO with a total volume of 2 ml. Then the complexes were titrated with LPS at room temperature and their emission spectra were measured after 2 min of each addition. A plot of emission intensity of the complexes at their emission maxima as a function of LPS concentration gave a linear dynamic response. The limit of detection (LOD) of LPS by using the complexes was determined by using the following formula: $C_{LOD} = 3\sigma/S$, where, σ is the standard deviation (SD) obtained from six independent measurements of emission intensity of the iridium complexes in aqueous media without any LPS and S is the slope obtained after linear fitting of the titration curves. For instance, the values of σ and S were calculated to be 4.00 and 0.255, respectively for 50 μ M solution of complex **Ir1** with LPS according to Fig. 2b. Thus, the C_{LOD} value of LPS by using complex **Ir1** was determined to be 47 nM.

Characterization of LPS-Ir(III) aggregates by DLS

The hydrodynamic diameters (d) of the iridium complexes and LPS-Ir(III) aggregates were determined by DLS. For this, a 50 μ M aqueous solution of the iridium complexes with and without 3 μ M of LPS was taken in a cuvette with a total volume of 2 ml containing 1% DMSO. DLS was operated at 25 $^{\circ}$ C using a 4 mW laser at a 632.8 nm wavelength and a detection angle of 90 $^{\circ}$.

Transmission electron microscopy (TEM) studies

A 50 μ M aqueous solution of the iridium complexes containing 1% MeCN was treated with 3 μ M of LPS in a final volume of 1 ml and incubated for 5 min. 10 μ l of aliquots from this reaction were deposited on carbon coated copper grids (CF 200 CU, Electron Microscopy Sciences, USA) and allowed for slow evaporation at room temperature overnight. The dried sample was imaged using a JEOL JEM-1400 electron microscope. As a control, 10 μ l of the complex solutions were taken out from the 50 μ M solution for TEM imaging.

Effect of pH on LPS detection

The phosphorescence emission intensity of the iridium complexes (**Ir1** and **Ir2**) for the detection of LPS was examined in HEPES buffer (10 mM) in the pH range from 4 to 9 at room temperature. For this, the emission intensity of the complexes (50 μ M) with and without LPS (6 μ M) between pH 4 and 9 was determined using a SpectraMax[®] M2e fluorescence microplate reader (Molecular Devices LLC, USA). The measurements were

performed in 96 well-plates with an excitation wavelength of 425 nm, a 630 nm cut-off and an emission wavelength of 720 nm and 688 nm for **Ir1** and **Ir2**, respectively.

Naked eye detection of bacteria

E. coli and *S. aureus* bacteria were grown in their mid-log phase and 10⁸ CFU per ml of bacteria were harvested, washed and resuspended in endotoxin-free water. Then, 400 μ M of the **Ir1** complex was added to 500 μ l of the bacterion suspension in an Eppendorf. The reaction mixture was monitored and the time point of aggregation was reported. Furthermore, the aggregation was also visualized using fluorescence microscopy (an Olympus IX73 inverted microscope fitted with an Orca Flash 4.0 CMOS camera from Hamamatsu). The fluorescence image was recorded at 40X magnification using long pass filter range of 595/50 nm.

Author contributions

P. K. S. conceptualized the project and designed the experiments, and wrote and edited the manuscript. Ar. G. synthesized and characterized the compounds and performed the experiments with LPS, analyzed the experimental data, and wrote the manuscript. Aj. G. assisted in the synthesis and characterization of compounds and studies with LPS. P. P. performed the experiments in bacteria, and wrote and edited the manuscript.

Conflicts of interest

There are no conflicts to declare.

Acknowledgements

P. K. S. acknowledges MHRD-STARS (project code: MoE-STARS/STARS-1/374) for financial support. We thank AIRF, JNU for the instrumentation facilities. Ar. G. acknowledges the UGC for a fellowship. Aj. G. gratefully acknowledges MHRD-STARS for a fellowship.

References

- 1 D. Li, B. Kumari, J. M. Makabenta, A. Gupta and V. Rotello, *Nanoscale*, 2019, **11**, 22172–22181.
- 2 P. Prasad, A. Gupta and P. K. Sasmal, *Chem. Commun.*, 2021, **57**, 174–186.
- 3 C. R. Raetz and C. Whitfield, *Annu. Rev. Biochem.*, 2002, **71**, 365–700.
- 4 B. Beutler and E. T. Rietschel, *Nat. Rev. Immunol.*, 2003, **3**, 169–176.
- 5 A. Tyndall and V. Pistoia, *Nat. Med.*, 2009, **15**, 18–20.
- 6 P. Prasad, S. Sachan, S. Suman, G. Swayambhu and S. Gupta, *Langmuir*, 2018, **34**, 7396–7403.

- 7 P. F. Roslansky and T. J. Novitsky, *J. Clin. Microbiol.*, 1991, **29**, 2477–2483.
- 8 P. Rajapaksha, A. Elbourne, S. Gangadoo, R. Brown, D. Cozzolino and J. Chapman, *Analyst*, 2019, **144**, 396–411.
- 9 P. M. Fratamico, *Mol. Cell. Probes*, 2003, **17**, 215–221.
- 10 J. Sun, A. R. Warden, J. Huang, W. Wang and X. Ding, *Anal. Chem.*, 2019, **91**, 7524–7530.
- 11 Y. Zhu, N. Gasilova, M. Jović, L. Qiao, B. Liu, L. T. Lovey, H. Pick and H. H. Girault, *Chem. Sci.*, 2018, **9**, 2212–2221.
- 12 A. K. Boardman, W. S. Wong, W. R. Premasiri, L. D. Ziegler, J. C. Lee, M. Miljkovic, C. M. Klapperich, A. Sharon and A. F. Sauer-Budge, *Anal. Chem.*, 2016, **88**, 8026–8035.
- 13 L. Yu, Y. Qiao, L. Miao, Y. He and Y. Zhou, *Chin. Chem. Lett.*, 2018, **29**, 1545–1559.
- 14 S. Sargazi, I. Fatima, M. H. Kiani, V. Mohammadzadeh, R. Arshad, M. Bilal, A. Rahdar, A. M. Díez-Pascual and R. Behzadmehr, *Int. J. Biol. Macromol.*, 2022, **206**, 115–147.
- 15 H. Zhu, J. Fan, J. Du and X. Peng, *Acc. Chem. Res.*, 2016, **49**, 2115–2126.
- 16 W. Lei, G. Jiang, Q. Zhou, Y. Hou, B. Zhang, X. Cheng and X. Wang, *Sens. Actuators, B*, 2012, **166–167**, 853–858.
- 17 F. Liu, J. Mu, X. Wu, S. Bhattacharjya, E. K. L. Yeow and B. Xing, *Chem. Commun.*, 2014, **50**, 6200–6203.
- 18 S. Voss, R. Fischer, G. Jung, K.-H. Wiesmüller and R. Brock, *J. Am. Chem. Soc.*, 2007, **129**, 554–561.
- 19 J. Wu, A. Zawistowski, M. Ehrmann, T. Yi and C. Schmuck, *J. Am. Chem. Soc.*, 2011, **133**, 9720–9723.
- 20 M. Lan, J. Wu, W. Liu, W. Zhang, J. Ge, H. Zhang, J. Sun, W. Zhao and P. Wang, *J. Am. Chem. Soc.*, 2012, **134**, 6685–6694.
- 21 L. Zeng, J. Wu, Q. Dai, W. Liu, P. Wang and C.-S. Lee, *Org. Lett.*, 2010, **12**, 4014–4017.
- 22 J. D. Luo, Z. L. Xie, J. W. Y. Lam, L. Cheng, H. Y. Chen, C. F. Qiu, H. S. Kwok, X. W. Zhan, Y. Q. Liu, D. B. Zhu and B. Z. Tang, *Chem. Commun.*, 2001, 1740–1741.
- 23 J. Li, J. X. Wang, H. X. Li, N. Song, D. Wang and B. Z. Tang, *Chem. Soc. Rev.*, 2020, **49**, 1144–1172.
- 24 X. L. Cai and B. Liu, *Angew. Chem., Int. Ed.*, 2020, **59**, 9868–9886.
- 25 H. Wang and G. Liu, *J. Mater. Chem. B*, 2018, **6**, 4029–4042.
- 26 J. Mei, Y. Huang and H. Tian, *ACS Appl. Mater. Interfaces*, 2018, **10**, 12217–12261.
- 27 Q. Peng and Z. Shuai, *Aggregate*, 2021, **2**, e91.
- 28 S. Ma, S. Du, G. Pan, S. Dai, B. Xu and W. Tian, *Aggregate*, 2021, **2**, e96.
- 29 X. Liu, Z. Yang, W. Xu, Y. Chu, J. Yang, Y. Yan, Y. Hu, Y. Wang and J. Hua, *J. Mater. Chem. C*, 2019, **7**, 12509–12517.
- 30 X. Hu, L. Jiang, H. Ye, B. Zhu and G. Niu, *Dyes Pigm.*, 2021, **194**, 109653.
- 31 G. Jiang, J. Wang, Y. Yang, G. Zhang, Y. Liu, H. Lin, G. Zhang, Y. Li and X. Fan, *Biosens. Bioelectron.*, 2016, **85**, 62–67.
- 32 Y. Tang, A. Kang, X. Yang, L. Hu, Y. Tang, S. Li, Y. Xie, Q. Miao, Y. Pan and D. Zhu, *Sens. Actuators, B*, 2020, **304**, 127300.
- 33 P. Alam, C. Climent, P. Alemany and I. R. Laskar, *J. Photochem. Photobiol., C*, 2019, **41**, 100317.
- 34 Y. Zhu, C. Xu, Y. Wang, Y. Chen, X. Ding and B. Yu, *RSC Adv.*, 2017, **7**, 32632–32636.
- 35 M. Gao, Q. Hu, G. Feng, N. Tomczak, R. Liu, B. Xing, B. Z. Tang and B. Liu, *Adv. Healthcare Mater.*, 2015, **4**, 659–663.
- 36 G. Feng, C.-J. Zhang, X. Lu and B. Liu, *ACS Omega*, 2017, **2**, 546–553.
- 37 S. Gao, X. Yan, G. Xie, M. Zhu, X. Ju, P. J. Stang, Y. Tian and Z. Niu, *Proc. Natl. Acad. Sci. U. S. A.*, 2019, **116**, 23437–23443.
- 38 S. K. Sheet, B. Sen, S. K. Patra, M. Rabha, K. Aguan and S. Khatua, *ACS Appl. Mater. Interfaces*, 2018, **10**, 14356–14366.
- 39 N. Jain, P. Alam, I. R. Laskar and J. Panwar, *RSC Adv.*, 2015, **5**, 61983–61988.
- 40 A. Gupta, P. Prasad, S. Gupta and P. K. Sasmal, *ACS Appl. Mater. Interfaces*, 2020, **12**, 35967–35976.
- 41 L. Xu, P. Deng, W. Song, M. Liu, M. Wang, Y. Yu and F. Wang, *ACS Mater. Lett.*, 2023, **5**, 162–171.
- 42 P. Y. Ho, S. Y. Lee, C. Kam, J. Zhu, G. G. Shan, Y. Hong, W. Y. Wong and S. Chen, *Adv. Healthcare Mater.*, 2021, **10**, 2100706.
- 43 Y. Pei, Y. Sun, M. Huang, Z. Zhang, D. Yan, J. Cui, D. Zhu, Z. Zeng, D. Wang and B. Tang, *Biosensors*, 2022, **12**, 1104.
- 44 H. Shi, Y. Wang, S. Lin, J. Lou and Q. Zhang, *Dalton Trans.*, 2021, **50**, 6410–6417.
- 45 K. Qiu, Y. Chen, T. W. Rees, L. Ji and H. Chao, *Coord. Chem. Rev.*, 2019, **378**, 66–86.
- 46 A. Gupta, T. Adarsh, V. Manchanda, P. K. Sasmal and S. Gupta, *Dalton Trans.*, 2023, **52**, 1188–1192.
- 47 G. Kumari, A. Gupta, R. K. Sah, A. Gautam, M. Saini, A. Gupta, A. K. Kushawaha, S. Singh and P. K. Sasmal, *Adv. Healthcare Mater.*, 2023, **12**, 2202411.
- 48 L. Di, Y. Xing, Z. Yang, C. Qiao and Z. Xia, *Sens. Actuators, B*, 2023, **375**, 132898.
- 49 H. Chen, S. Li, M. Wu, Kenry, Z. Huang, C. S. Lee and B. Liu, *Angew. Chem., Int. Ed.*, 2020, **59**, 632–636.
- 50 H. Huang, B. Yu, P. Zhang, J. Huang, Y. Chen, G. Gasser, L. Ji and H. Chao, *Angew. Chem., Int. Ed.*, 2015, **54**, 14049–14052.
- 51 E. Zhao, Y. Chen, S. Chen, H. Deng, C. Gui, C. W. Leung, Y. Hong, J. W. Lam and B. Z. Tang, *Adv. Mater.*, 2015, **27**, 4931–4937.